JOURNAL OF THE KOREAN ASTRONOMICAL SOCIETY
29: 255~268, 1996

PHOTOMETRY AND SPECTROSCOPY OF THE SPIRAL GALAXY NGC7678

ANN, HONG -BAE AND KIM, JEONG -MI
Department of Earth Sciences, Pusan National University, Pusan 609-735, Korea
(Received September 9, 1996; Accepted October 4, 1996)

ABSTRACT

We present VR CCD photometry and long-slit spectroscopy of a late type spiral galaxy NGC 7678. The grey scale images and isophotal maps illustrate the presence of a weak bar from which spiral arms emerge. There are many HII regions along the spiral arms, but bright giant HII regions are more concentrated in the massive southern arm. The bright compact nucleus of NGC 7678 is bluer than bulge and bar. The spectral features of the nucleus and HII regoins are very similar but the nuclear spectra shows higher [NII]λ6583/H_α than those of the HII regions. The nucleus of NGC 7678 seems to be intermediate type between HII region nulcei and LINERs by the ratio of [NII]λ6583/H_α, but it is more likely to be HII region-like nucleus if we consider the [SNII]λ6716,6731/H_α together. The star formation rate is estimated to be about 0.2 $M_\odot$ yr^{-1} based on the H_α flux.

I. INTRODUCTION

NGC 7678 is a peculiar spiral galaxy which has a massive spiral arm in the south of the center of the galaxy. Owing to its pronounced asymmetry of the spiral arms, it was classified as an interacting galaxy by Vorontsov-Velyaminov (1977) although there seems to be no apparent companion galaxy. Dahari (1985) considered NGC 7678 as a weakly interacting galaxy and assigned interaction class (IAC) of 2 to it. However, the southern spiral arm of the galaxy is so enormously massive that there might be strong interactions at least in the past.

In spite of the peculiarities of the morphology of NGC 7678 there had been little detailed surface photometry until quite recently. The first detailed surface photometry was made by Kent (1984) who showed that the luminosity distribution of NGC 7678 can not be approximated by ellipses. Recent BVRI and H_α surface photometry of Wozniak et al. (1995) also showed that the isophotes of NGC 7678 are too distorted to be approximated by ellipses.

NGC 7678 has been known to have nuclear emission lines which are different from those of Seyfert galaxies. According to Dahari (1985)'s nuclear emission type (NET), which is defined by the line ratios, [OIII]λ5007/H_β, [NII]λ6583/H_α, and [OI]λ6300/H_α, the nucleus of NGC 7678 has intermediate spectral properties between HII region nuclei and LINERs.

In this paper we present the results of V and R band surface photometry of NGC 7678 along with long-slit spectroscopy of the nucleus and one giant HII region located in the southern arm. The main aim of the present study is to clarify the nature of the nucleus of NGC 7678 by comparing the spectral properties of the nucleus and the HII region of NGC 7678. In the next section we describe the obserbations and data reduction, and in §III we present the results of the present study. Discussions on the physical properties of NGC 7678 based on our spectra are described in §IV, and a brief summary and conclusions are given in the last section.

II. OBSERVATION AND DATA REDUCTION

(a) Images

The observations of NGC 7678 were made on the night of 29 July 1992 with a FA 2048 CCD (2048 × 2048, 15^2 μm^2 pixels) attached at the modified Newtonian focus of the 1.8 m Plaskett Telescope of Dominion Astrophysical Observatory (DAO). The gain and readout noise of the CCD were $9.1e^{-1}$/ADU and $3e^{-1}$, respectively. The images

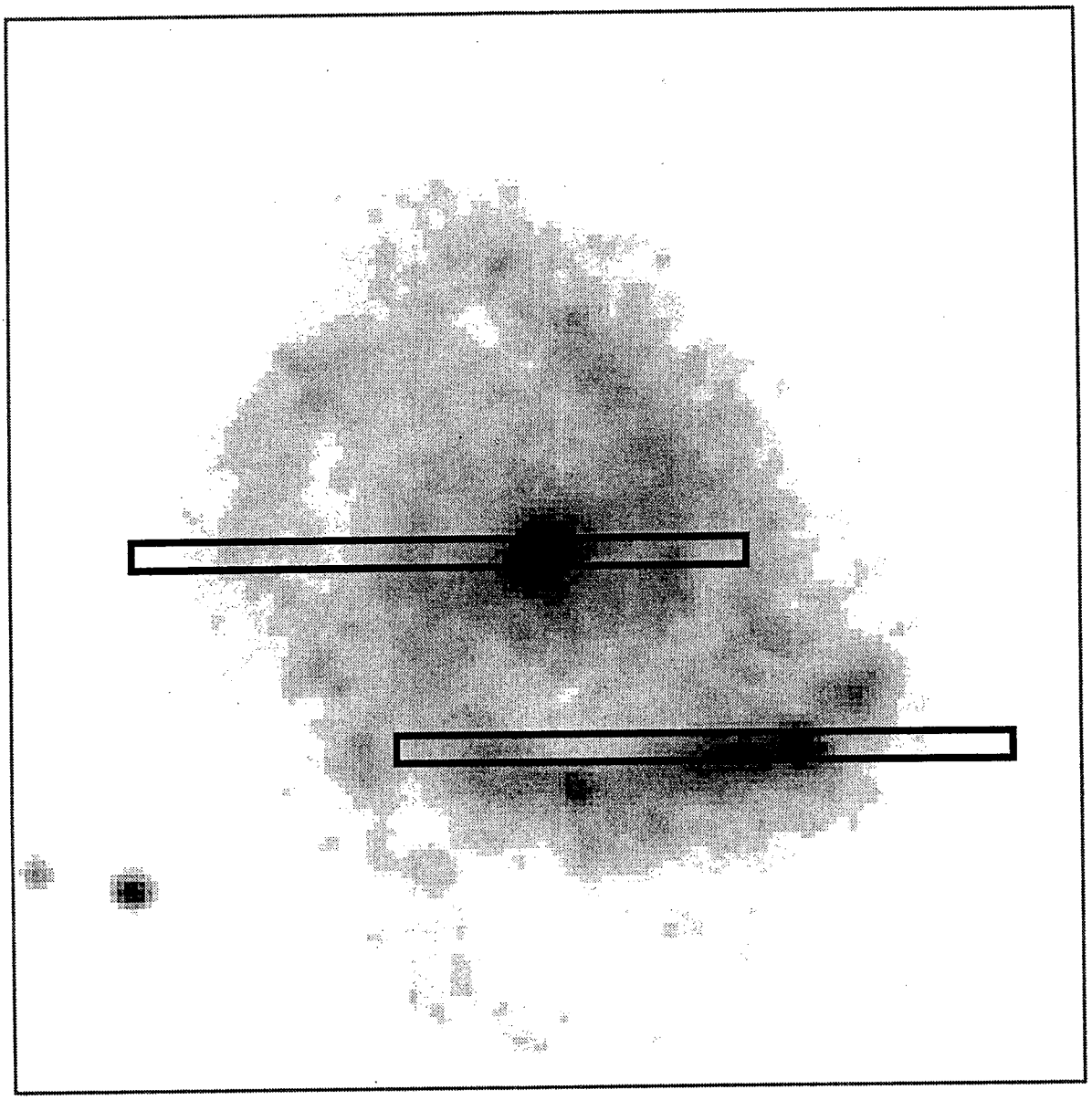

Fig. 1. V-band gray scale image of NGC 7678. There are many HII regions along the spiral arms which emerge from the end of bar. Two slit positions are shown.

were recorded with 2×2 on-chip binning which gives the image scale of $0.''65$/pixel. The images were obtained with Johnson-Cousin V and R filters with exposure times of 120s and 180s, respectively. The seeing, defined as the full width at half maximum (FWHM) of a star profile was about $2''$. Bias frames were obtained before and after the observations, and the flat field images were taken during twilight. Several standard stars in M92 were observed for the transformation of the instrumental magnitudes to the standard photometric system.

The raw data were processed with CCDRED package in the IRAF software systems. Flat-fielding was performed by subtracting a mean bias frame, and dividing by a normalized flat field. The flat fielded frames of galaxy images were subtracted and devided by sky frames which were obtained by fitting the sky regions surrounding the galaxy images, by using SPIRAL package which is developed at Kiso observatory for galaxy surface photometry. A variable width Gaussian smoothing was performed on the resulting image frames to increase the S/N of the luminosity distribution of the galaxy, especially in the outer part.

The absolute calibration of the galaxy photometry was done by determining the sky brightness from the photom-

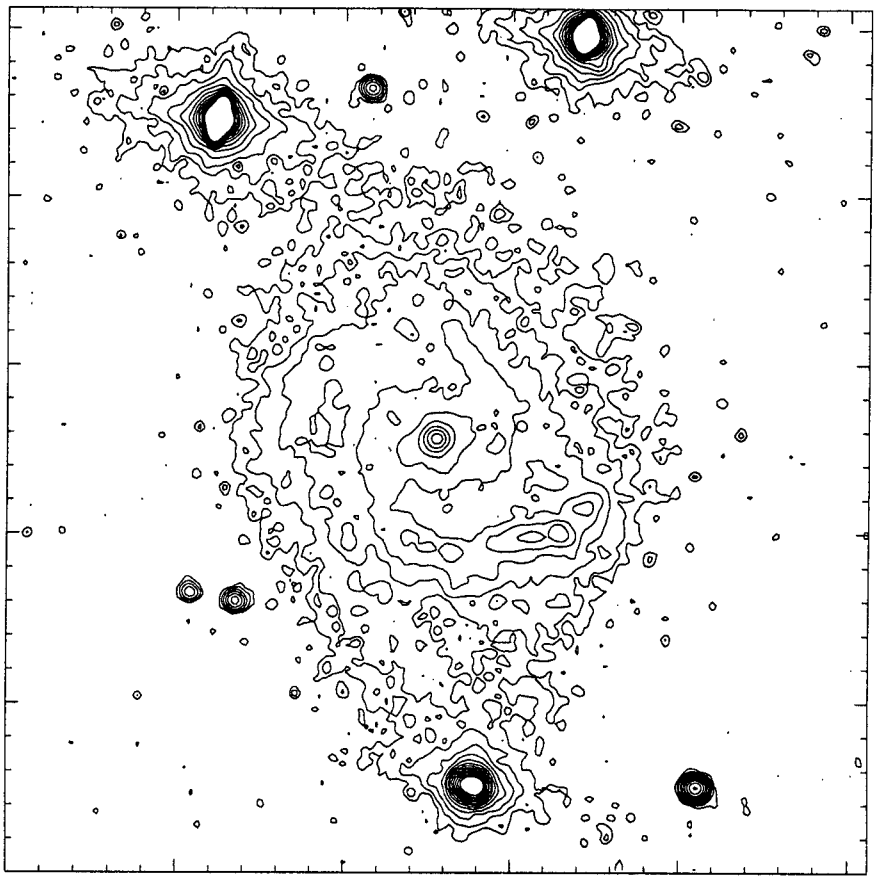

Fig. 2. V-band image of NGC 7678. Isophotes are seperated by 0.5 mag arcsec^{-2}, and the faint contour is 3 mag arcsec^{-2} fainter than the sky brightness of 20.26 mag arcsec^{-2}. North is up and East is to the left.

etry of the standard stars. The instrumental magnitudes of the standard stars were corrected for the atmospheric extinction and transformed to the standard systems using the following equations:

$$V = v + 0.04(V - R) + 20.54$$

$$R = r + 0.39(V - R) + 20.38.$$

Here v and r are instrumental magnitudes and V and R are standard manitudes by Heasley and Christian (1986), respectively. The sky brightness in V and R are 20.26 mag arcsec^{-2} and 19.43 mag arcsec^{-2}, respectively.

(b) Spectra

Long-slit spectra of the nuclear region and the brightest HII region on the southern spiral arm of NGC 7678 were obtained at DAO using PM512 CCD (512 × 512, 20^2 μm^2 pixels) and the Cassegrain spectrograph installed on the 1.8m Plaskett telescope on the night of 3 September 1993. A $60'' \times 2''$ slit was used with a 600 lines mm^{-1} grating. The dispersion was 30 Å/ mm which corresponds to 0.6Å/pixel. The scale along the slit was $0.''8$/pixel after on chip binning by 2 along the slit direction. The observations covered the wavelength ranges of λ6500Å – λ6820Å with a spectral resolution of 2.7 Å. The slit was set across the nucleus and the brightest HII region, along the east-west direction. The slit across the nucleus covered the bar-like structure whose position angle is about 90°. Figure 1 shows the locations and orientations of the slit projected on the grey scale map of NGC 7678 in V-band.

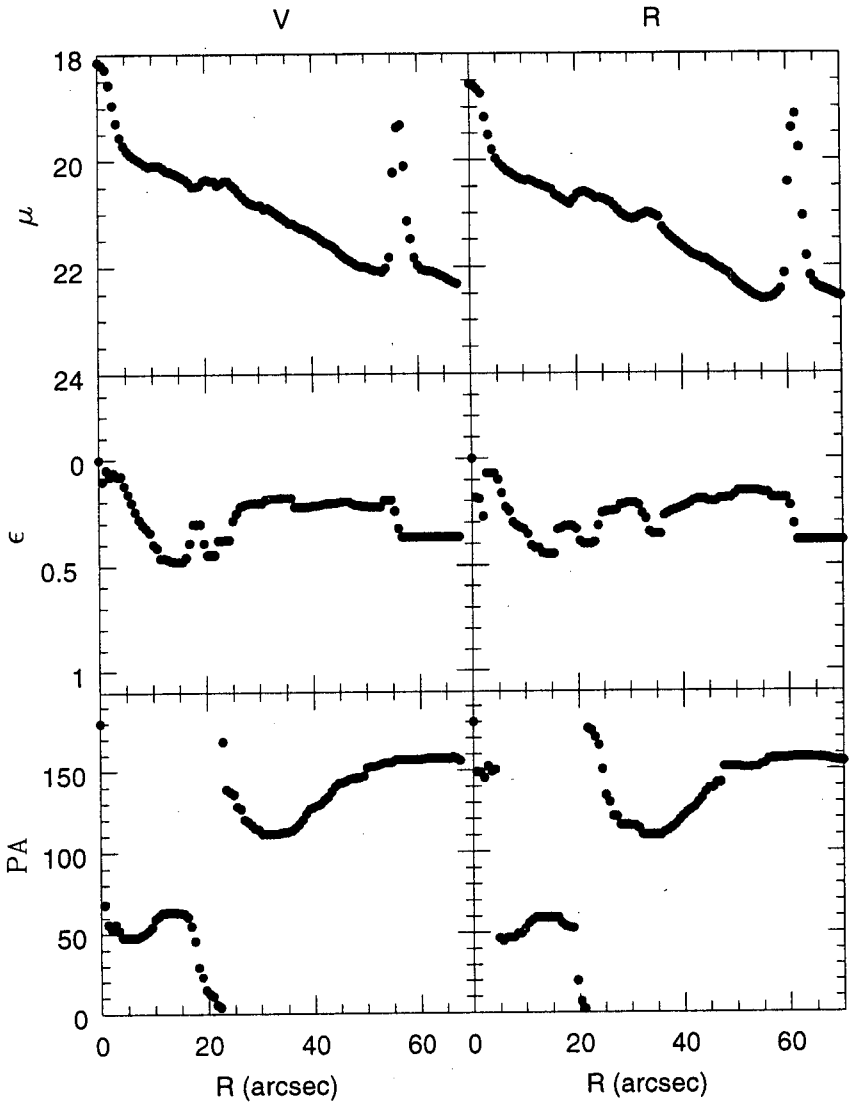

Fig. 3. Surface brightness (μ), ellipticities (ϵ), and position angle (PA) along the the major axis of NGC 7678. The left panel is for the V-band image, and the right panel is for the R-band.

Standard reduction procedures in IRAF software system (CCDRED and LONGSLIT) were used for the reduction of the long-slit data. A mean bias frame and dark frames were subtracted from the raw data before flat fielding. The flat fields from diffuse lamp and twilight sky were used to make an illumination corrected flat field. Wavelength calibration using the spectra of Fe/Ar lamp was performed before the atmospheric extinction correction and flux calibration. We used the spectra of standard star HR 718 which was observed on the same night for flux calibration. We extracted spectra from the long-slit images using APEXTRACT package in IRAF software systems.

III. RESULTS

(a) Imaging

i) Morphology

The grey scale image in Figure 1 and the isophotes of NGC 7678 in Figure 2 clearly show the morphological properties which are characterized by a small nucleus, a weak bar, and asymmetric spiral arms with several bright

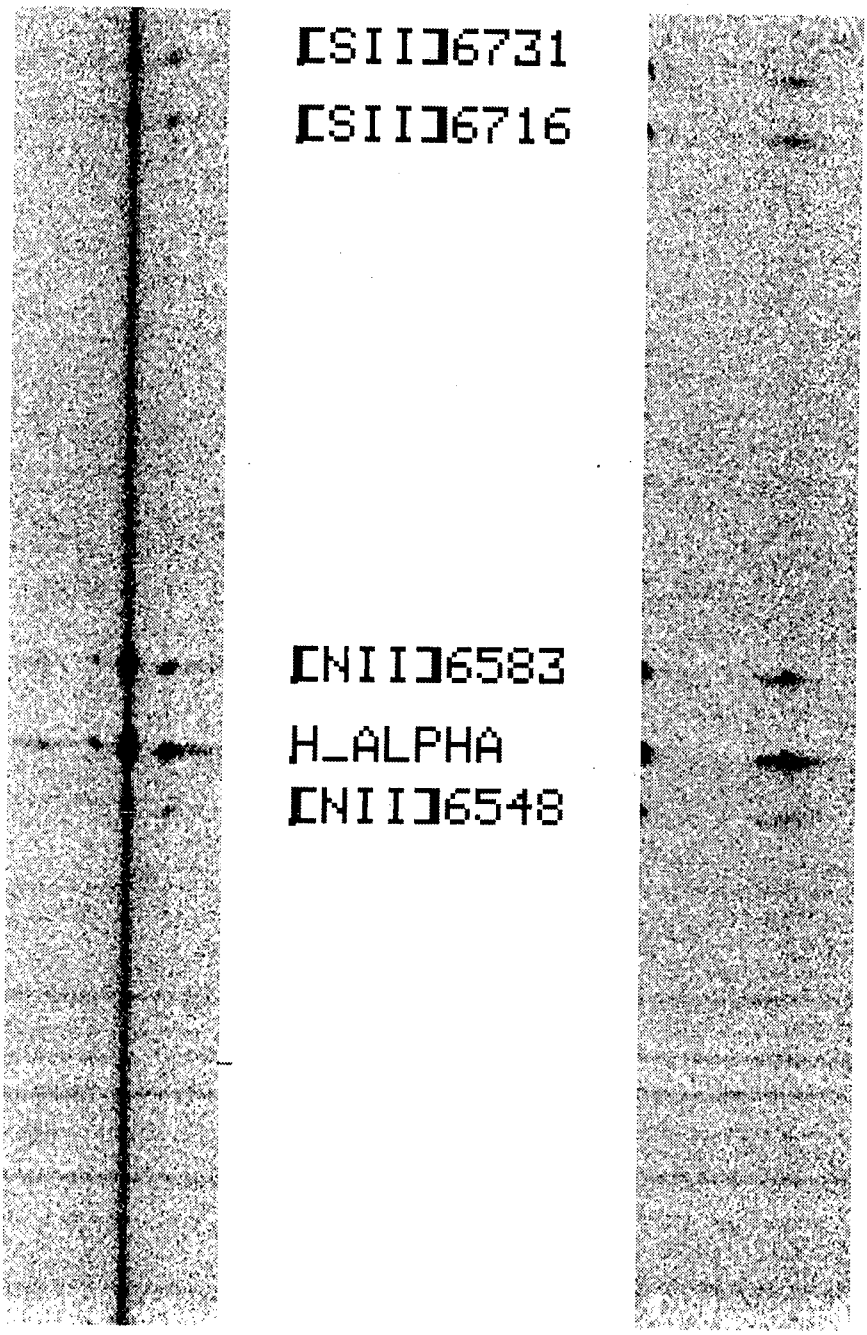

Fig. 4. Long-slit images of NGC 7678. The left panel represents the nuclear spectra and the right panel represents the giant HII region spectra.

giant HII regions on the southern arm. There are many HII regions along the spiral arms that emerge from the ends of the bar. The HII regions are noticeable by the luminosity enhancements which are represented by dark patchiness in the grey scale maps or locally closed contours in the isophotal maps, along the spiral arms. Close look at the well contrasted grey scale maps shows that the two spiral arms are quite symmetric until revolution of $\sim 90°$. The northern spiral arm extends smoothly to the PA of $\sim 230°$, which resemble typical spiral arms of late type galaxies. The pronounced asymmetry is due to the southern arm which seems to be much more massive than the northern arm. The abnormally large and bright HII regions in the southern arm indicate strong star forming activity induced by interactions with other galaxies. It is quite plausible that the brightest giant HII region in the southern arm is a

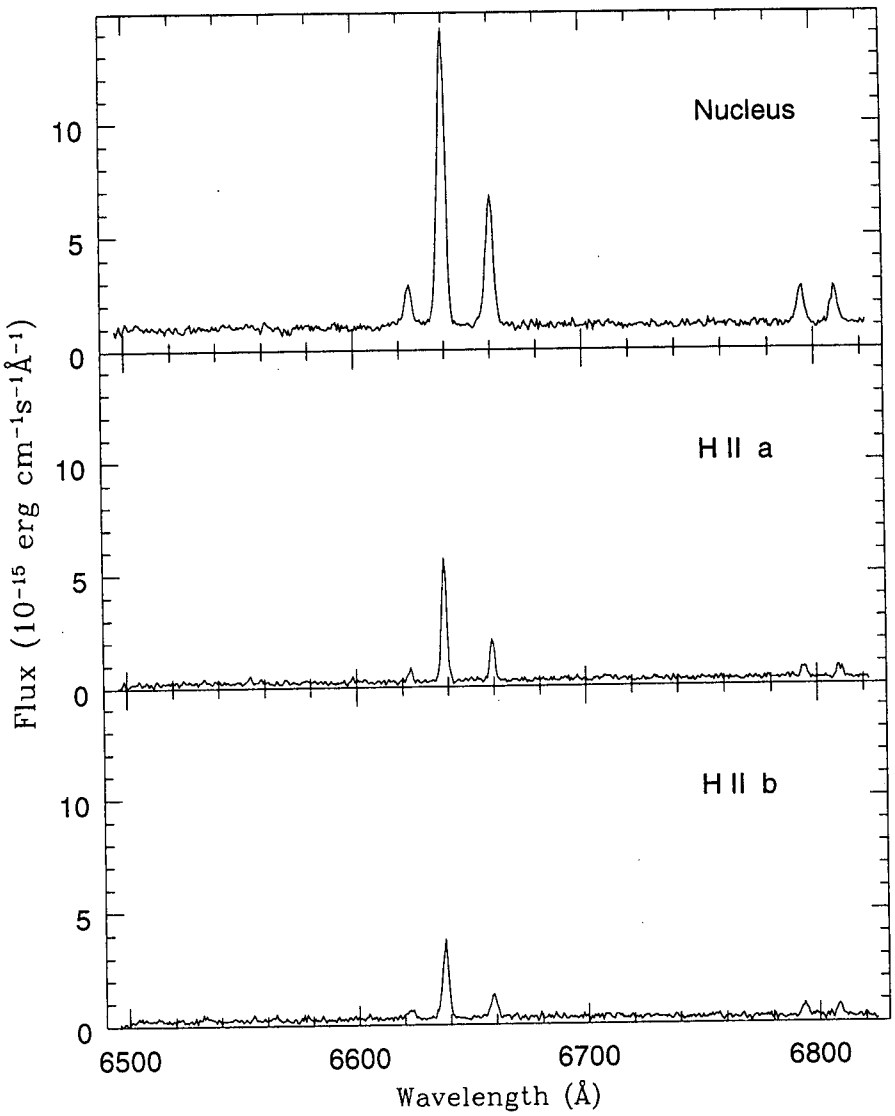

Fig. 5. Spectra of the nucleus and HII regions. Middle panel for the HII region in the inner spiral arm and bottom panel for the giant HII region in the southern arm.

relic of a satellite galaxy which was merged in the past. The absence of the spiral arms in the direction of PA $\geq 270°$ may reflect strong interaction with other galaxies near the southern arm. Due to several bright forground stars, the outer boundary of the disk is difficult to discern. There seems to be no difference in the luminosity distributions between the V and R band images.

ii) Luminosity Distribution

We applied ellipse fitting to the observed luminosity distributions of NGC 7678 to analyze the luminosity profiles and the geometric properties of the galaxy. Figure 3 shows variations of surface brightness (μ), ellipticities (ϵ), and the position angles (PA) along the major axis of the galaxy. The steep gradients of the luminosity profile inside the bulge reflect the small bulge and the bright nucleus of the galaxy. The shallow gradients of the luminosity profile in the inner disk are due to the luminosities in the massive spiral arms. The small bump at $r \sim 10''$ in the surface brightness distributions reflects the luminosity enhancement caused by the HII regions near the ends of the bar, while the broad bump at $r \sim 25''$ is due to the giant HII regions in the southern arm. The bright points at $r \sim 58''$ are foreground stars. Due to complexity caused by the bar and the massive spiral arm, it was impossible to decompose the luminosity profiles into bulge and disk components. However, it is apparent that the bright compact

Table. 1. Equivalent width and emission line fluxes of the Nucleus of NGC 7678

	[NII]λ6548		H_α		[NII]λ6853		[SII]λ6716		[SII]λ6731	
R	EW	Flux	EW	Flux	EW	Flux	EW	Flux	EW	Flux
-3	0.97	0.33	15.18	5.07	8.54	2.96	2.72	1.01	2.57	0.93
-2	4.10	1.91	26.34	12.20	13.90	6.50	4.12	2.09	3.07	1.53
-1	6.44	4.27	39.47	26.19	18.84	12.58	5.19	3.63	5.10	3.40
0	7.14	6.58	48.83	44.06	23.16	20.54	6.79	6.09	6.10	5.45
1	7.49	7.58	55.00	54.35	26.57	25.30	7.50	7.15	7.10	6.82
2	7.65	6.72	55.03	48.41	26.71	22.46	7.63	6.57	6.59	5.81
3	6.76	4.25	48.28	30.29	23.45	14.54	5.95	3.84	6.08	3.92
4	6.01	2.47	33.81	13.83	17.37	7.27	4.32	1.93	5.21	2.32

Note. EW unit = Å. Flux unit = 10^{-15}ergs cm^{-2} s^{-1}. R is distance from the nucleus in unit of 0.″8. The minus sign represents the eastern distance.

nucleus is bluer than bulge and bar.

The ellipticity varies smoothly inside the bar whose ellipticity is $\sim$ 0.45. This means that the axial ratio of the bar is 0.55. The ellipticity of the disk whose PA is 10° is 0.18. The abrupt changes in PA at $r \sim 24''$ is due to spiral arms which emerge from the end of the bar.

(b) Spectroscopy

i) Long-Slit Images

Figure 4 presents the long-slit images of the of NGC 7678. The left image is the long-slit image for the slit set to cross the nucleus and the right one is for the slit set to cross the giant HII region in the massive southern spiral arm. The images in Figure 4 were trimmed to cut the bad images near the east edge of the slit. The cosmic rays were removed from the images. As shown in Figure 4, there are emission lines of H_α, [NII]λ6548,6583, and [SII]λ6716,6731, along with several night sky lines. The emission lines outside the nucleus in the left image seem to come from the HII regions located near the ends of the bar where the inner spiral arms begin to emerge. The emission lines from the HII region located at $\sim 13''$ west of the nucleus seem to be stronger than those from the HII region located at $\sim 10''$ east of the nucleus. The emission lines of [NII]λ6548 and [SII]λ6716,6731 are too weak to be visible in the east HII region. However, the H_α lines come from the entire disk except for the bulge/bar region. The strong H_α emission at $\sim 26''$ east of the nucleus comes from an HII region of the outer spiral arm which emerges from the west end of the bar, as shown in Figure 1. The strong emission lines in the right image come from the giant HII region in the massive southern arm. The strength of the emission lines from the central part of the giant HII region in the southern arm is stronger than those from the HII regions in the inner spiral arms. but the spatial extent of the HII region is much larger than that of the nucleus and the HII regions in the inner arms. The strongly emitting region near the east edge of the slit is another bright HII region located in the southern arm.

ii) Spectra

In Figure 5 we present the nuclear spectrum of NGC 7678 along with the spectra of the HII regions of the inner spiral arms and the massive southern arm. The middle panel shows the spectra of the HII region in the inner spiral arms (HIIa) and the bottom represents the spectra of the HII region in the southern spiral arm (HIIb). The spectra were extracted from the long-slit images with an aperture of 2.″4 which corresponds to a linear size of $\sim$580 pc assuming that distance of the galaxy is 50 Mpc (H_o = 75 km s^{-1} Mpc^{-1}). The S/N of continuum flux is $\sim$ 10 for the nuclear spectra and $\sim$ 4 for those of the HII regions. However, the S/N of the emission lines, which is defined

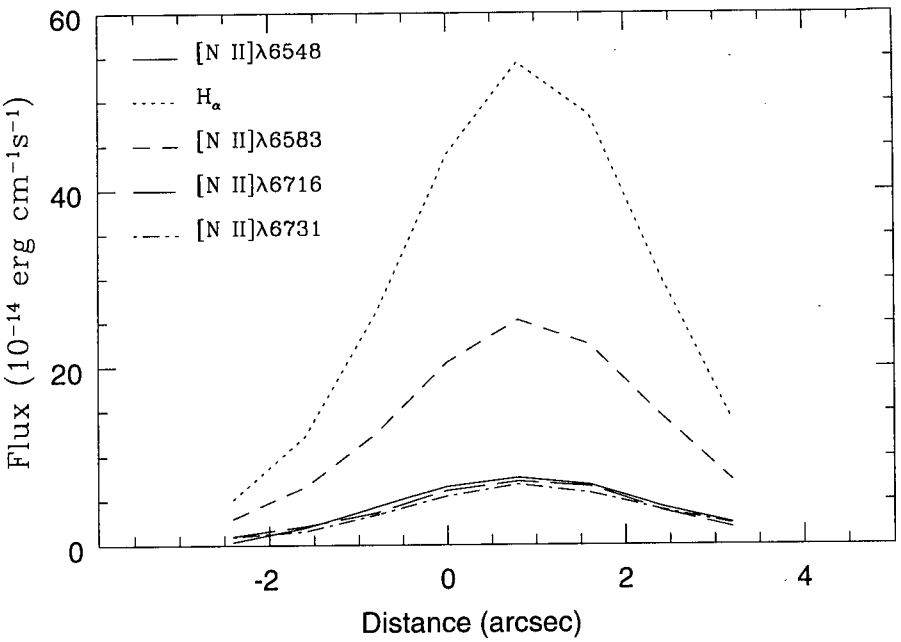

Fig. 6. Spatial distribution of the emission line fluxes from the nucleus. Notice the offset of the position of the maximum flux from the center of the galaxy.

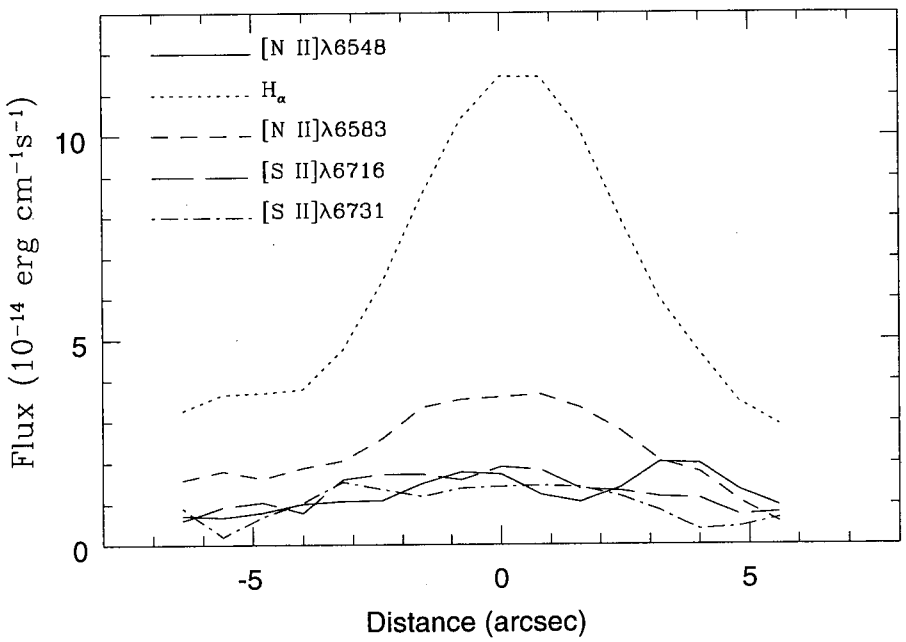

Fig. 7. Spatial distribution of the emission line fluxes from the giant HII region in the southern arm.

by the ratio of the flux of the emission line to the rms scatter of the continuum near the emission line, is greater than 20 for the faintest lines in Figure 5. Because of high resolution ($\sim$ 2.7Å), there is no blending between H_α and [NII]λ6548 lines. The spectral features of the nucleus and the two HII regions (HIIa, HIIb) are similar except for the fluxes of the emission lines. However, there seems to be slight difference in the relative strength of [SII]λ6716 and [SII]λ6731 lines between the nucleus and the HII regions.

To analyze the spatial variation of the spectral properties within the nucleus and the giant HII region in the

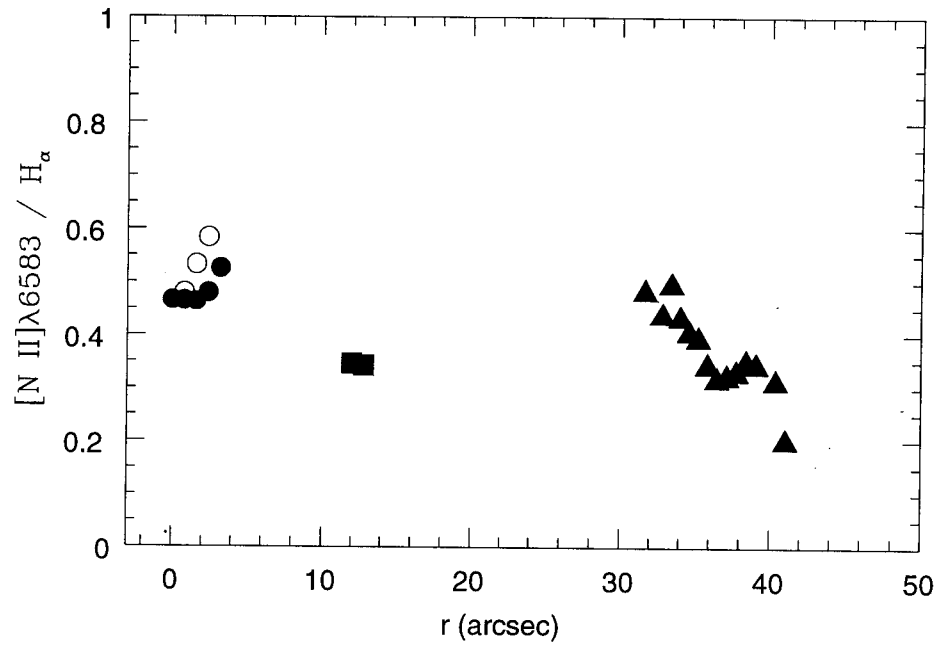

Fig. 8. Spatial distribution of [NII]λ6583/H$_\alpha$ for the nucleus and the HII regions. The circles represent the spectra for the nuclear region, open circle for the apertures in the east part and the closed circle for the west part of the nucleus. The rectangle and triangle represent the spectra for the HII regions in the inner spiral arms and the massive southern arm, respectively.

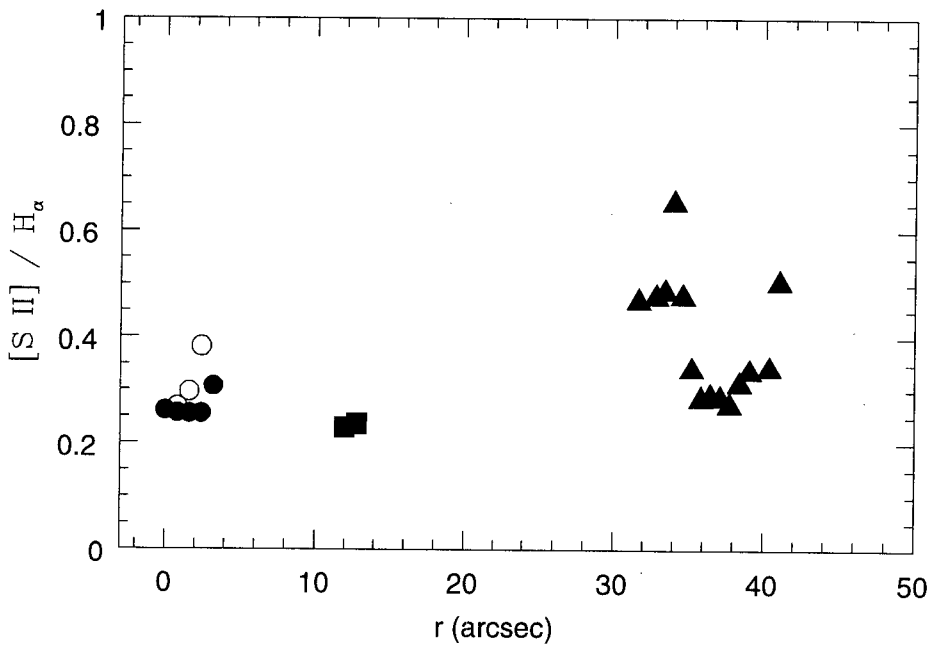

Fig. 9. Spatial distribution of [SII]/H$_\alpha$ for the nucleus and the HII regions. The meaning of the symbols is the same as that of Fig. 8.

southern spiral arm, we extracted spectra of the nucleus and the HII region with an apertures of 2.″4, seperated by 0.″8. For the nucleus we also extract the whole aperture (7.″2 × 2″) spectrum which was obtained by summing all the spectra of the nuclear region into a single spectrum. We used the SPLOT task in IRAF to analyze the spectral features of the extracted spectra. We measured the line fluxes and equivalent widths of the H$_\alpha$, [NII]λ6548,6583,

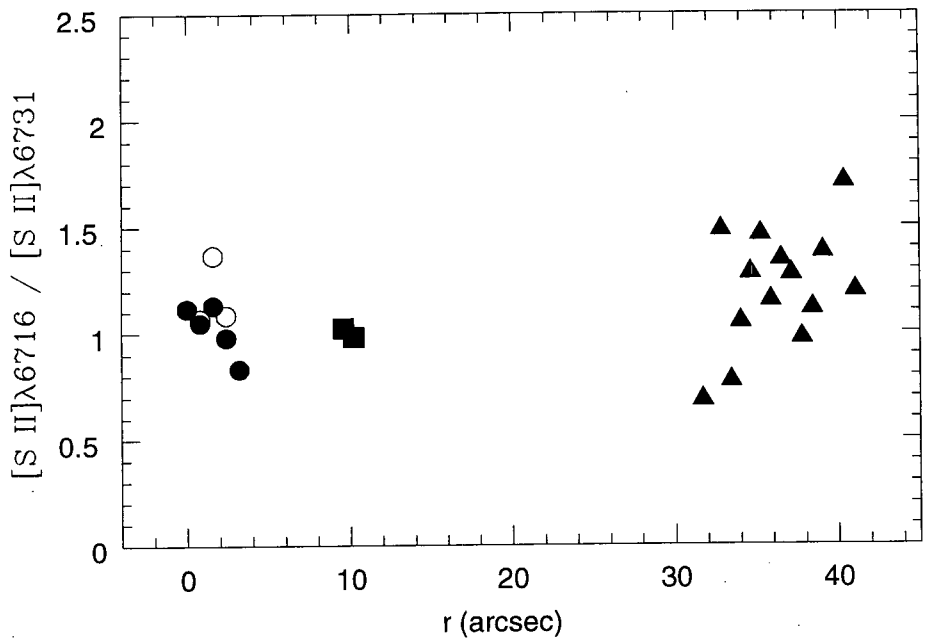

Fig. 10. Spatial distribution of [SII]λ6716/S[II]λ6731. The meaning of the symbols is the same as that of Fig.8.

and [SII]λ6716,6731 by Gaussian fitting which was provided in the SPLOT package. We do not need deblending algorithms to measeure the line fluxes due to relatively high spectral resolution. The line fluxes and equivalent widths of the extracted spectra whose S/N is greater than 10 are listed in Table 1 for the nuclear spectra and in table 2 for the giant HII region in the southern arm.

iii) Spatial Distribution of Emission Lines

As shown in Figure 4 the continuum emission is concentrated in the circumnuclear region. Most of the continuum emission comes from the central 4″ while the emission lines come from more extended regions. Figure 6 shows the spatial distribution of the emission lines fluxes as a function of distance from the nucleus. The minus sign in this figure represents the eastern region. The maximum of the line emission is offset $\sim 1''$ to the west of the nucleus whose position is determined by the position of maximum in the continuum distribution. Similar offset has been found in the spectra of a starburst galaxy NGC 7714 (Gonzalez-Delgado *et al.* 1995). H_α lines are strongest throughout the emitting regions but the H_α fluxes rapidly decline outward. The [NII]λ6583 lines also decline outward quite rapidly but all the other lines vary very smoothly throughout the nuclear region.

As shown in Figure 7, the strength of the emission lines from the giant HII region in the southern arm also varies along the slit. The spatial distribution of H_α fluxes from the HII region is very symmetric for the inner part of the HII region. The distances in abscissa are measured from the position of the maximum flux in the emission lines. The maximum H_α flux of the HII region is $\sim$ 20% of that of the nucleus but it is similar to the H_α flux of the HII regions in the inner spiral arms. The [NII]λ6583 lines vary more smoothly than the H_α lines in the central part of the HII region.

iv) Spatial Variation of Emission Line Ratios

Figure 8 presents the spatial variation of the emission line ratios of [NII]λ6583/H_α for the nucleus and the HII regions. The circles represent the spectra for the nuclear region, open circle for the apertures in the east part and the closed circle for the west part of the nucleus. The rectangle and triangle represent the spectra for the HII regions in the inner spiral arms and the massive southern arm, respectively. We fixed the the size of aperture at 2.″4. There seems to be a marginal trend of decreasing [NII]λ6583/H_α ratio with the distance from the center of the galaxy.

Table. 2. Equivalent width and emission line fluxes of the giant HII region in the southern arm

	[NII]λ6548		H_α		[NII]λ6853		[SII]λ6716		[SII]λ6731	
R	EW	Flux	EW	Flux	EW	Flux	EW	Flux	EW	Flux
-8	3.10	0.73	13.87	3.27	6.70	1.57	3.16	0.62	4.96	0.91
-7	2.92	0.70	16.46	3.66	7.89	1.79	4.94	0.94	1.04	0.19
-6	3.36	0.81	16.27	3.70	6.82	1.61	5.98	1.05	4.05	0.71
-5	4.18	1.02	16.03	3.79	7.92	1.87	4.05	0.80	6.35	1.04
-4	4.33	1.08	19.65	4.76	8.62	2.05	7.69	1.59	7.44	1.52
-3	4.12	1.09	25.86	6.40	10.06	2.58	10.06	1.71	8.18	1.34
-2	6.23	1.49	35.03	8.53	12.88	3.34	8.10	1.72	5.85	1.18
-1	6.93	1.77	40.90	10.38	13.23	3.54	6.83	1.57	6.11	1.37
0	6.91	1.72	45.85	11.44	12.77	3.60	8.71	1.89	6.38	1.41
1	4.56	1.22	43.73	11.43	13.21	3.66	8.56	1.82	6.51	1.43
2	4.07	1.05	40.23	10.15	12.22	3.33	6.88	1.36	7.61	1.40
3	5.66	1.38	32.20	7.98	10.51	2.77	6.76	1.31	6.38	1.18
4	8.91	2.01	25.73	6.01	7.94	2.05	6.33	1.17	4.60	0.85
5	8.88	1.97	21.92	4.68	8.41	1.77	6.26	1.13	2.12	0.38
6	5.13	1.33	13.43	3.48	4.20	1.08	3.80	0.75	2.29	0.44
7	3.77	0.97	11.41	2.92	2.32	0.58	4.67	0.80	3.88	0.67

Note. EW unit = Å. Flux unit = 10^{-15}ergs cm^{-2} s^{-1}. R is distance from the center in unit of 0.″8. The minus sign represents the eastern distance.

The ratio of [NII]λ6583/H$_\alpha$ from the aperture which entirely covers the nucleus is $\sim$ 0.5. This indicates the nucleus of NGC 7678 is intermediate between the HII region nuclei and LINER (Dahari 1985). However, [SII]/H$_\alpha$ of the nucleus implies that the nucleus of NGC 7678 is closer to the HII region-like nuclei. In Figure 9, we present the spatial variation of [SII]/H$_\alpha$ for the nucleus and the HII regions. The meaning of the symbols is the same as that of Figure 8.

IV. DISCUSSION

(a) Spatial Variation of Electron Density

The electron densities of the emitting regions can be inferred by measuring the observed [SII]λ6716/S[II]λ6731. Figure 10 shows the spatial variation of [SII]λ6716/S[II]λ6731 as a function of radius from the center of the galaxy. The [SII]λ6716/λ6731 of the nucleus is $\sim$ 1 which is slightly less than those of the giant HII regions. We derived the electron density from the [SII]λ6716/S[II]λ6731 by using the calculation of Osterbrock (1989). The derived electron densities at the nucleus and the central region of the HII region in the southern arm are 500 cm^{-3} and 100 cm^{-3}, respectively, with the assumption of the electron temperature of 10000 K. The electron density at the HII region in the inner arm is found to be 550 cm^{-3}. The electron density of the nucleus of NGC 7678 is somewhat larger than the average densities of HII region nuclei (280 cm^{-3}), LINERs (350 cm^{-3}), and Seyfert 2 galaxies (430 cm^{-3}) (Veilleus *et al.* 1995), but quite small compared to the electron densities of the two starburst galaxies He 2-10 (1000 cm^{-3}) and Mrk52 (770 cm^{-3}) (Sugai & Taniguchi 1992). However, it well lies in the ranges of 100-1000 cm^{-3} for nuclear HII regions (Kennicutt *et al.* 1989). The electron densities of the giant HII region is also comparable to typical values of 10-100 cm^{-3} for disk HII regions (Kennicutt *et al.* 1989). The electron densities of the HII regions

in the inner spiral arms are too high compared with those of the disk HII regions.

(b) Star Formation Rates

It is generally assumed that the strong H_α emissions in interacting galaxies are caused by the enhanced birthrates of massive stars triggered by interactions. We calculate the star formation rates using the H_α luminosity. We adopt the following calibration by Bushouse (1987)

$$SFR(H_\alpha) = 7.07 \times 10^{-42} L(H_\alpha)\, M_\odot\ yr^{-1},$$

where $L(H_\alpha)$ is the H_α luminosity which is derived from the galactic extinction corrected H_α flux,

$$F_c(H_\alpha) = F_{obs}(H_\alpha) 4 \times 10^{0.969 E_{B-V}}.$$

Here E_{B-V} was determined by using the value of A_B=0.11 in NED (NASA/IPAC Extragalaxy Database).[]NED is operated by the Jet Propulsion Laboratoty, California Institute of Technology, under contract with the National Aeronautics and Space Adminstration. Assuming 50 Mpc for the distance of NGC 7678, the $L(H_\alpha)$ of NGC 7678 from the whole aperture ($7.''2 \times 2''$) spectra of the nucleus is estimated to be 2.52×10^{40} erg s^{-1}. The resulting SFR(H_α) is $\sim$ 0.2 $M_\odot$ yr^{-1}. Derived SFR(H_α) of the nucleus of NGC 7678 is 3 and 7.5 times larger than the average SFRs for the interacting galaxies and isolated galaxies derived by Bushouse (1987). Because our spectra and the calibration of Bushouse (1987) have not been corrected for internal reddening, which is at least E(B-V) $\sim$ 0.3 for the interacting galaxies (Bushouse 1987), the actual SFR(H_α) in the nucleus of NGC 7678 is at least two times higher than the derived value. The SFR derived from the UV luminosity by Donas *et al.* (1987) is 5.34 $M_\odot$ yr^{-1}, which is a factor of 20 higher than ours. However, if we consider that we did not correct the internal reddening on the observed H_α fluxes due to lack of H_β fluxes in our spectra, the actual difference is not so large, because our estimate of SFR is considered to be a lower limit. Moreover, the IMF used for the derivation of SFR from H_α flux by Bushouse (1987) is different from that used by Donas *et al.* (1987). Bushouse (1987) used Salpeter (1955) IMF with lower and upper mass cutoff, 0.1 $M_\odot$ and 100 $M_\odot$, respectively, while Donas *et al.* (1987) used the IMF obtained by Lequeux (1979) with lower and upper mass cutoff of 0.007 $M_\odot$ and 120 $M_\odot$, respectively. The Lequeux (1979) IMF gives a factor of $\sim$ 2 higher SFR than the Salpeter IMF.

It is a complicate problem to compare SFRs among galaxies, because IMFs may be different in interacting galaxies and normal galaxies (Gehrz *et al.* 1983; Auguarde & Lequeux 1985; Auguarde & Lequeux 1986). However, the fact that the SFR of the nuclear region of NGC 7678 is higher than the mean SFR of interacting galaxies implies that the nucleus of NGC 7678 is quite active. Another evidence for active star formation in the nucleus of NGC 7678 is the large EW of H_α lines: EW(H_α) = 39 Å for the nuclear region ($7.''2 \times 2''$). This is larger than the mean value for 19 HII region nuclei (EW(H_α) = 31Å) (Kennicutt *et al.* 1989), and slightly smaller than that for luminous infrared galaxies with IAC = 2 (EW(H_α) = 42Å) (Veilleus *et al.* 1995). Because the linear size of the region covered by our nuclear spectra is nearly the same as those of Veilleus *et al.* (1995) and Kennicutt *et al.* (1989), the large EW(H_α) in the nucleus of NGC 7678 implies that this region is more active than the ordinary HII region nuclei.

The SFRs for the giant HII region is 0.08 $M_\odot$ yr^{-1} for the $16'' \times 2''$ aperture and 0.06 for $7.''2 \times 2''$ aperture, respectively. The former aperture covers all the regions where H_α fluxes can be measured. The star formation rates per unit area (SFR_a) for the giant HII region is 4.2×10^{-8} $M_\odot$ yr^{-1} pc^{-2} for large aperture and 6.7×10^{-8} $M_\odot$ yr^{-1} pc^{-2} for the small aperture, respectively. These are a factor of 3 lower than the mean SFR_a of the four HII regions in a Seyfert galaxy NGC 1667 (Radovich & Rafanelli 1996) for spectra with $7.''2 \times 2''$ aperture. The SFR_a of the nuclear region of NGC 7678 with the apertures of $2.''4 \times 2''$ and $7.''2 \times 2''$ is 4.25×10^{-7} $M_\odot$ yr^{-1} pc^{-2}, 2.13×10^{-7} $M_\odot$ yr^{-1} pc^{-2}, respectively.

(c) Nuclear Type

It is generally assumed that HII region nuclei can be distinguished from LINERs or Seyfert galaxies by emission line ratios (Osterbrock 1989). The most widely used method of classfying nuclear type is to plot three diagnostic

[1

diagrams of [NII]λ6583/H_α versus [OIII]λ5007/H_β, [SII]λ6716,6731/H_α vrsus [OIII]λ5007/H_β, and [OI]λ6300/H_α versus [OIII]λ5007/H_β (Liu & Kennicutt 1995). However, we can not use these diagnostics due to narrow spectral coverage of our spectra. Instead, we used the line ratios of [NII]λ6583/H_α to determine the NET of NGC 7678 using Dahari (1985)'s criteria. The value of 0.47 for [NII]λ6583/H_α is just the value for the intermediate type between HII region nuclei and LINERs, which is consistent with the classification of Dahari (1985). But if we use the [NII]λ6583/H_α and [SII]λ6716,6731/H_α together, the nucleus of NGC 7678 seems to be more HII region-like because the values of [NII]λ6583/H_α and [SII]λ6716,6731/H_α are less than the lower limit of LINERs in the diagnostic diagrams of [NII]λ6583/H_α versus [OIII]λ5007/H_β, [SII]λ6716,6731/H_α vrsus OIII]λ5007/H_β (Osterbrock 1989). The average emission line ratios for the star forming and Seyfert 2 galaxies by Storchi-Bergman *et al.* (1995) and star forming galaxies by McQuade *et al.* (1995) support the HII region-like nature of the nucleus of NGC 7678.

V. SUMMARY AND CONCLUSIONS

VR CCD imaging and long-slit spectroscopy from λ6500 Å to λ6850 Å have been obtained for the late type spiral galaxy NGC 7678. The morphology from V and R-band images indicates that the galaxy experienced strong interactions which induced active star formation in the nucleus and the giant HII regions in the southern arm. The absence of the spiral arms in the direction of PAs $\geq 270°$ may reflect the strong interaction with other galxies near the southern arm. It is quite plausible that the brightest HII region in the massive southern arm may be a relic of satellite galaxy which was merged in the past. The offset of the location of the maximum H_α flux from the nucleus supports the hypothesis that satellite galaxies were merged into the galaxy.

The nuclear emission lines are confined to a narrow region compared to the giant HII region. The H_α flux of the nucleus is a factor of 5 larger than those of the HII regions in the inner arm and in the southern arm for the same aperture of $2.''4 \times 2''$. However, the spectral features of the nuclear region and the HII regions are found to be similar except for the slight difference in the line ratio of [NII]λ6583/H_α. The [NII]λ6583/H_α of the nuclear spectra is a factor of 1.4 larger than that of the giant HII region. There seem to be slight gradients in [NII]λ6583/H_α and [SII]/H_α along the radius. The ratios of [NII]λ6583/H_α and [SII]λ6716,6731/H_α from the nuclear spectra show that the nucleus of NGC 7678 seems to be closer to the HII region-like nucleus. The densities determined from the [SII]λ6716/[SII]λ6731 are 500 cm^{-3}, 100 cm^{-3}, and 550 cm^{-3} for the the nucleus, HII region in the inner spiral arm, and the giant HII region, respectively. The density of the nucleus is somewhat larger than the average density of of HII region nuclei, LINERs, and Seyfert 2 galaxies observed by Veilleus *et al.* (1995), but it is within the ranges of 100-1000 cm^{-3} for typical nuclear HII regions (Kennicutt *et al.* 1989).

The SFR in the nucleus of NGC 7678 is estimated to be ~ 0.2 $M_\odot$ yr^{-1}, based on the H_α flux. It is 3 times and 7.5 times higher than the average SFRs for the interacting galaxies and isolated galaxies (Bushouse 1987). But the present SFR estimated from the H_α flux is a lower limit of the actual SFR in the nucleus of the galaxy. The SFR_a of the giant HII region is founded to be 6.7×10^{-8} $M_\odot$ yr^{-1} pc^{-2} for $7.''2 \times 2''$ aperture, which is a factor of 3 lower than the mean SFR_a of the four HII regions in a Seyfert galaxy NGC 1667 (Radovich & Rafanelli 1996).

ACKNOWLEDGEMENTS

We would like to thank Dr. H. M. Lee for careful reading the manuscripts and valuable comments. H. B. Ann is grateful to the hospitalities provided by DAO. This work was supported in part by the Basic Science Research Institute Program, Ministry of Education, BSRI-95-5411.

REFERENCES

Auguarde, R., & Lequeux, J. 1985, A&A, 147, 273.
Bushouse, H. 1987, ApJ, 320, 49.
Dahari, 1985, ApJS, 57, 643.

Donas, J., Deharveng, J. M., Laget, M., Milliard, B., & Huguenin, D.1987, A&A, 180, 12.
Gehrz, R. D., Sramek, R. A., & Weedman, D. W. 1983, ApJ, 267, 551.
Gonzalez-Delgado, R.M., Perez, E., Diaz, A. I., GArcia-Varga, M. L., Terlevich, E., & Vilchez, J. M. 1995, ApJ, 439, 604.
Heasley, J. N., & Christian, C. A. 1986, ApJ, 307, 738.
Kennicutt, R. C., Keel, W. C., & Blaha, C. A. 1989, AJ, 97, 1022.
Kent, S. M. 1984, ApJS, 56, 105.
Lequeux, J. 1979, A&A, 80, 35.
Liu, C. T., & Kennicutt, R. C. 1995, ApJ, 450, 547.
Osterbrock, D. E. 1989, Astrophysics of Gaseous Nebulae and Active Galactic Nuclei (University Science Books, Mill Valley)
McCal, M. L., Rybski, P. M., & Shields, G. A. 1985, ApJS, 57, 1.
McQuade, K., Calzetti, D., & Kinney, A. ApJS, 97, 331.
Radovich, M., & Rafanelli, P. 1996, A&A, 306, 97.
Salpeter, E. 1955, ApJ, 121, 161.
Storchi-Bergmann, T., Kinney, A., & Challis, P. 1995, ApJS, 98,
Sugai,H., & Taniguchi, Y. AJ, 103, 1470. 103.
Veilleux, S., Kim, D.-C., Sanders, D. B., Mazzarella, M., & Soifer, B. T. 1995, ApJS, 98, 171.
Vorontosov-Velyaminov, B. 1977, A&AS, 28, 1.
Wozniak, H., Friedli, D., Martinet, L., Martin, P.,& Bratschi, P. 1995, A&AS, 111, 115.